Zero expiratory pressure and low oxygen concentration promote heterogeneity of regional ventilation and lung densities

J. B. Borges[1,2], L. Porra[3,4], M. Pellegrini[5], A. Tannoia[5], S. Derosa[5], A. Larsson[1], S. Bayat[6], G. Perchiazzi[1,5] and G. Hedenstierna[7]

[1]Hedenstierna Laboratory, Department of Surgical Sciences, Section of Anaesthesiology & Critical Care, Uppsala University, Uppsala, Sweden
[2]Pulmonary Divison, Heart Institute (Incor) Hospital das Clínicas da Faculdade de Medicina da Universidade de São Paulo, Brazil
[3]Department of Physics, University of Helsinki, Helsinki, Finland
[4]Helsinki University Central Hospital, Helsinki, Finland
[5]Department of Emergency and Organ Transplant, Bari University, Italy
[6]Inserm UMR1105 and Pediatric Lung Function Laboratory, CHU Amiens, Université de Picardie Jules Verne, Amiens, France
[7]Hedenstierna Laboratory, Department of Medical Sciences, Clinical Physiology, Uppsala University, Uppsala, Sweden

Correspondence
João Batista Borges, Department of Surgical Sciences, Section of Anaesthesiology & Critical Care, Uppsala University. Hospital, 751 85, Uppsala, Sweden.
E-mail: joao.batista_borges@surgsci.uu.se

Conflicts of interest
None.

Funding
Swedish Research Council, K2015-99X -22731-01-4. The Swedish Heart and Lung Foundation. Picardie Regional Council. School of Anesthesia and Intensive Care Medicine, Bari University, Italy. Centre of Innovative Technologies for Signal Detection and Processing (TIRES), Bari University, Italy.

The work was carried out in the European Synchrotron Radiation Facility, Grenoble, France.

Submitted 5 August 2015; accepted 11 February 2016; Submission 20 January 2016;

Citation
Borges JB, Porra L, Pellegrini M, Tannoia A, Derosa S, Larsson A, Bayat S, Perchiazzi G, Hedenstierna G. Zero expiratory pressure and low oxygen concentration promote heterogeneity of regional ventilation and lung densities. Acta Anaesthesiologica Scandinavica 2016

doi: 10.1111/aas.12719

Background: It is not well known what is the main mechanism causing lung heterogeneity in healthy lungs under mechanical ventilation. We aimed to investigate the mechanisms causing heterogeneity of regional ventilation and parenchymal densities in healthy lungs under anesthesia and mechanical ventilation.

Methods: In a small animal model, synchrotron imaging was used to measure lung aeration and regional-specific ventilation ($s\dot{V}$). Heterogeneity of ventilation was calculated as the coefficient of variation in $s\dot{V}$ ($CV_{s\dot{V}}$). The coefficient of variation in lung densities (CV_D) was calculated for all lung tissue, and within hyperinflated, normally and poorly aerated areas. Three conditions were studied: zero end-expiratory pressure (ZEEP) and F_IO_2 0.21; ZEEP and F_IO_2 1.0; PEEP 12 cmH_2O and $F_IO_2$1.0 (Open Lung-PEEP = OLP).

Results: The mean tissue density at OLP was lower than ZEEP-1.0 and ZEEP-0.21. There were larger subregions with low $s\dot{V}$ and poor aeration at ZEEP-0.21 than at OLP: 12.9 ± 9.0 vs. $0.6 \pm 0.4\%$ in the non-dependent level, and 17.5 ± 8.2 vs. $0.4 \pm 0.1\%$ in the dependent one ($P = 0.041$). The $CV_{s\dot{V}}$ of the total imaged lung at PEEP 12 cmH_2O was significantly lower than on ZEEP, regardless of F_IO_2, indicating more heterogeneity of ventilation during ZEEP (0.23 ± 0.03 vs. 0.54 ± 0.37, $P = 0.049$). CV_D changed over the different mechanical ventilation settings ($P = 0.011$); predominantly, CV_D increased during ZEEP. The spatial distribution of the CV_D calculated for the poorly aerated density category changed with the mechanical ventilation settings, increasing in the dependent level during ZEEP.

Conclusion: ZEEP together with low F_IO_2 promoted heterogeneity of ventilation and lung tissue densities, fostering a greater amount of airway closure and ventilation inhomogeneities in poorly aerated regions.

Editorial comment: what this article tells us
This study explored the forces that lead to heterogeneity in lung aeration. In this animal model with healthy lungs, zero airway pressure and lower inspired oxygen content contributed to inhomogeneous ventilation in more poorly aerated lung regions.

Acta Anaesthesiologica Scandinavica
AN INTERNATIONAL JOURNAL OF ANAESTHESIOLOGY AND INTENSIVE CARE, PAIN AND EMERGENCY MEDICINE

Worldwide, more than 230 million patients undergoing major surgery each year require general anesthesia and mechanical ventilation,[1] and 20–30% of these patients are at intermediate to high risk for postoperative pulmonary complications,[2] which affect clinical outcomes.[3] Mechanical ventilation can initiate ventilator-induced lung injury (VILI)[4,5] and contribute to extrapulmonary organ dysfunction.[6] Up to 25% of patients with normal lungs when placed on mechanical ventilation for 2 days or longer will develop mild acute respiratory distress syndrome (ARDS), with 60–80% of those progressing to moderate to severe ARDS.[5,7,8] A lung-protective ventilation strategy in intermediate- and high-risk patients undergoing major abdominal surgery improved clinical outcomes.[9] A strategy to prevent VILI and ARDS is obviously desirable,[5,10–13] but to achieve this, a better understanding of the primary mechanisms of VILI and ARDS development in healthy lungs under general anesthesia and mechanical ventilation is needed.

There is a growing recognition that ARDS following mechanical ventilation occurs often as a two-hit phenomenon.[11] A predisposing condition, such as an inflammatory endothelial (e.g. sepsis) or epithelial (e.g. aspiration) injury, is followed by a second insult that is predominantly mechanical in nature, resulting in activation of primed neutrophils and progression to ARDS. Strategies targeting risk factor modification, that is, avoiding a second-hit in at-risk patients have the potential to reduce rates of ARDS[2,11] and may guide in implementing lung-protective ventilation strategies in patients without ARDS.[3,7,14–16]

A mechanical ventilation strategy that promoted stable lung recruitment and a more homogeneously ventilated lung, seems to have blocked early drivers of lung injury in normal lungs, preventing ARDS.[10] The strategy comprised the use of airway pressure release ventilation with a prolonged time spent at the upper pressure that recruited alveoli gradually over time, resulting in a more homogeneously ventilated lung. A decrease in ventilation heterogeneity was also argued to be the main mediator of beneficial effects in other studies, reducing volutrauma and atelectrauma.[5,10–13] But, it is not well known what is the main mechanism causing lung heterogeneity in healthy lungs under mechanical ventilation.

We hypothesized that low end-expiratory pressure together with low oxygen concentration would promote heterogeneity of regional-specific ventilation and lung tissue densities during mechanical ventilation. We therefore performed simultaneous measurements of parenchymal density, aeration, and regional-specific ventilation, by means of synchrotron radiation computed tomography imaging, aiming to investigate the main mechanisms causing lung heterogeneity in healthy lungs. To fulfill this goal, we assessed the interplay between gravitational level, PEEP, and inspiratory oxygen fraction (F_IO_2) on heterogeneity of regional ventilation and lung tissue densities.

Methods

The procedures for the animal care and the experiments were in accordance with the Directive 2010/63/EU of the European Parliament on the protection of animals used for scientific purposes,[17] and were approved by the Internal Evaluation Committee for Animal Welfare in Research of the European Synchrotron Radiation Facility, Grenoble, France.

Animal preparation

The experiments were performed on seven male New Zealand rabbits (2.8 ± 0.09 kg). A catheter (22 gauge) was inserted into the marginal ear vein under local anesthesia, using 5% topical lidocaine. Anesthesia was induced by the intravenous injection of 25 mg/kg of thiopental sodium. The animal was tracheotomized with a no. 3, Portex tube (Smiths Medical, Kent, United Kingdom). The left carotid artery and jugular vein were catheterized for blood gas measurements and for drug delivery, respectively. Anesthesia was then maintained with IV administration of 0.2 mg/kg/h of midazolam. After ensuring adequate anesthesia (no reaction by painful stimulation), continuous IV infusion of atracurium (1.0 mg/kg/h) was started. The animal was immobilized in the vertical, head-up position in a cylindrical polyvinyl chloride custom-made holder. Animals were in upright position throughout the study.

Pressure-controlled mechanical ventilation was delivered using a custom-made ventilator, described in detail previously.[18] The ventilator allowed synchronizing mechanical ventilation with the image acquisition. Wash-in image series of 15 images were recorded during inhalation of xenon (70%) and oxygen (30%), and ventilation was paused for 3 s for each image acquisition. The respiratory gas flow was monitored using a heated pneumotachometer (Hans Rudolph, Kansas City, MO, USA). The endotracheal pressure was monitored continuously. All monitored signals were amplified, digitized at 400 Hz (Powerlab, ADI Instruments, Oxfordshire, United Kingdom), and recorded on a computer.

Synchrotron radiation computed tomography imaging

The K-edge subtraction (KES) method is a lung imaging technique that uses synchrotron radiation to quantify the regional concentration of inhaled stable xenon within lung airspaces.[19,20] This technique allows simultaneous and quantitative measurements of regional-specific ventilation ($s\dot{V}$) as well as lung tissue density. A detailed description of the methodology and instrumental setup has been extensively discussed in previous studies.[19–22] This imaging technique uses dual X-ray beams at slightly different energies. X-rays from a synchrotron radiation source are required because, as opposed to standard X-ray sources, they allow the selection of monochromatic beams from the full X-ray spectrum while conserving enough intensity for imaging with sufficient temporal resolution. Two computed tomography images are thus simultaneously acquired after the inhalation of a xenon–oxygen gas mixture. Visualization and quantitative measurement of xenon within the airways is based on the property that the attenuation coefficient of xenon increases by a factor of 5.4 when the energy of the incident X-ray beam crosses the energy threshold of 34.56 keV, which is the xenon K-edge energy. Using the dual-energy KES imaging method, the densities due to tissue and xenon can be calculated separately in each voxel in the image, using a specifically developed computer algorithm[19] explained in detail elsewhere.[23] A 'xenon-density' image allows the direct quantitative measurement of contrast gas within the airways, and that of the regional gas volume. Dynamic KES imaging during xenon wash-in allows the measurement of regional $s\dot{V}$.[20] A 'tissue-density' image obtained from the same data allows quantitative measurement of the regional tissue density.

The experiments were performed at the Biomedical Beamline of the European Synchrotron Radiation Facility (ESRF, Grenoble, France). The monoenergetic beams with an energy difference of 250 eV were produced from the continuous synchrotron radiation spectrum by a bent silicon crystal. The beams focused and crossed at the animal position, beyond which they diverged and were recorded by a liquid nitrogen-cooled, high-purity germanium, dual-line detector (Eurisys Measure, Lingolsheim, France). The horizontal pixel size of the detector was 0.35 mm, and the vertical beam height was 0.7 mm. Image reconstruction was performed using the filtered-back-projection algorithm, using the Interactive Data Language (IDL; RSI, Boulogne- Billancourt, France).

Image analysis

Images were processed using the MatLab programming package (Mathworks Inc., Natick, MA, USA). Lung tissue was selected within the tissue-density computed tomography images, by region-growing segmentation. The volume of lung was then divided into four density categories: hyperinflated (comprising voxels with CT attenuation between: −1000 and −901 HU), normally aerated (between: −900 and −501 HU), poorly aerated (between: −500 and −101 HU), and non-aerated tissue (between: −100 and +100 HU). A coefficient of variation in lung densities (CV_D) was calculated for all of the lung tissue in the images, and within the normally aerated, hyperinflated, and poorly aerated lung regions.

The local specific ventilation or ventilation normalized to the gas volume within the voxel ($s\dot{V}$) was calculated from the time constant of the xenon wash-in using a single compartment model fit of xenon concentration vs. time.[22] A 5×5 pixel moving average window was applied to the xenon-density images prior to the model fit. The heterogeneity of ventilation was

calculated as the coefficient of variation in $s\dot{V}$ ($CV_{s\dot{V}}$) for all lung volume, and for areas within each density category contained in the image slice. In each $s\dot{V}$ image, the histogram of $s\dot{V}$ within normally aerated zones was calculated, and fit with a lognormal function. The median (μ) and standard deviation (σ) of the distribution were extracted from the fit. Normal, high, and low $s\dot{V}$ were defined with reference to the median value of each slice. The ventilated alveolar volume was defined as the volume of the ventilation image where $s\dot{V}$ was greater than the median of the distribution minus 2 standard deviations: $\mu-2\sigma$.

Measurements were made at two axial levels, one close to the diaphragm and one 4.5 ± 1.9 mm (mean ± standard deviation) in the cranial, vertical direction. In order to characterize the functional behavior of normally aerated, poorly aerated, and hyperinflated lung regions, the volume of lung within each density category was further divided into subcategories based on regional $s\dot{V}$: no ventilation, defined as: $s\dot{V} < 0.5$/min; low $s\dot{V}$: $0.5/\text{min} < s\dot{V} < (\mu-2\sigma)$; normal $s\dot{V}$: $s\dot{V} = \mu \pm 2\sigma$; high $s\dot{V}$: $(\mu + 2\sigma) < s\dot{V}$. Each subcategory was expressed as percentage of the total lung volume within the image slice.[24]

Study protocol

The horizontal X-ray beam used for functional imaging in this study required that the animal be positioned vertically. Although the vertical posture may slightly improve respiratory mechanics in the rabbit,[20] it has been already shown that it did allow assessment of the regional differences in lung function with respect to gravity.[24] The following procedure was performed to eliminate the effects of the head-up posture in terms of an increase in the end-expiratory lung volume and respiratory system compliance: (1) Scanogram in horizontal posture and assessment and notation of the diaphragm position; (2) Measurement of gastric pressure in supine posture; (3) Position vertically in the custom-made cylindrical polyvinyl chloride holder, exactly as during imaging; (4) Measurement of gastric pressure in vertical posture and inflation of inflatable cuff placed around the abdomen, in order to reach a gastric pressure equal to that in supine posture; (5) Check of diaphragmatic position; (6) Readjustment of cuff pressure if needed.

The animals were studied with the three following mechanical ventilation settings: PEEP = 12 cmH_2O and $F_IO_2 = 1.0$ (OLP = 'open lung PEEP'); PEEP = 0 cmH_2O and $F_IO_2 = 1.0$ (ZEEP-1.0); PEEP = 0 cmH_2O and $F_IO_2 = 0.21$ (ZEEP-0.21). The order of the three conditions was randomized (by random number), and upon each change in ventilator settings, 10 min were allowed for stabilization before imaging. A recruitment maneuver was performed before each step in the protocol in order to homogenize lung history. The settings of the recruitment maneuver were the following: pressure-controlled ventilation, PEEP = 18 cmH_2O, plateau pressure = 26 cmH_2O, $F_IO_2 = 1.0$, respiratory rate set at 30, inspiratory to expiratory ratio (I:E) 1:1, during 4 min.

After the recruitment maneuver, tidal volume was 3 to 5 ml/kg and respiratory rate set at 50–60/min.

Statistical analysis

With a study design where the animals served as their own controls, four animals were needed to obtain a power of 0.80 with a $P < 0.05$, with SD = ½ mean. The time frame available for our experiments allowed us to use seven animals, giving us sufficient statistical power. The scatters in the parameters were expressed by the SEM values. The Shapiro–Wilk test was used to test data for normality. When data were normally distributed, within-within-subjects ANOVA with two within-subject factors was applied. The two within-subject factors were the mechanical ventilation settings (three conditions: OLP/ZEEP-1.0/ZEEP-0.21) and gravity level (two conditions: non-dependent/dependent level). Where results showed significance, a Bonferroni adjustment for multiple tests was used for all pairwise comparisons. When the assumption of normality was violated, we used the Friedman test as non-parametric alternative. Pairwise planned contrasts were then performed with a Bonferroni correction for multiple comparisons.

A one-way repeated measures ANOVA was conducted to determine whether there were statistically significant differences in the gas exchange parameters over the three mechanical

ventilation settings. The gas exchange data was normally distributed, as assessed by Shapiro–Wilk test ($P > 0.05$). Where results showed significance, a Bonferroni adjustment for multiple tests was used for all pairwise comparisons.

The statistical analyses were conducted by SPSS (version 20.0.0). Statistical tests were carried out with the significance level set at P value less than 0.05.

Results

The gas exchange parameters and the respiratory variables are shown in Table 1.

At ZEEP, a heterogeneous distribution of mean density was seen at both horizontal image levels and the mean density increased from the non-dependent to dependent level ($P = 0.028$). The mean tissue density under OLP was lower than ZEEP-1.0 and ZEEP-0.21 ($P = 0.01$ and 0.012, respectively; Fig. 1A), was more homogeneous, was within the normally aerated density category and similar between non-dependent and dependent levels (Fig. 1A).

When calculated for all density categories together, the two gravity levels showed statistically significant changes in the CV_D over the different mechanical ventilation settings ($P = 0.011$, Fig. 1B): predominantly, CV_D increased during ZEEP.

There was a statistically significant interaction between gravity-dependence and mechanical ventilation settings in the CV_D calculated for the poorly aerated density category ($P = 0.013$, Fig. 1C), suggesting that the spatial distribution of the CV_D calculated for the poorly aerated density category changed with the mechanical ventilation settings, increasing in the dependent level during ZEEP.

Compared to OLP, the area of lung regions with both low $s\dot{V}$ and poor aeration was increased at ZEEP-0.21 ($P = 0.008$, 12.9 ± 9.0 vs. $0.6 \pm 0.4\%$ for the non-dependent level, and 17.5 ± 8.2 vs. $0.4 \pm 0.1\%$ for the dependent one). This is shown in Fig. 2.

Comparing the $CV_{s\dot{V}}$ for total lung area between OLP vs. ZEEP-0.21 and ZEEP-1.0 pooled together, there was a statistically significant difference indicating more heterogeneity of ventilation during ZEEP irrespective of F_IO_2 (0.23 ± 0.03 vs. 0.54 ± 0.37, $P = 0.049$).

Figure 3 shows representative tissue density and $s\dot{V}$ images at OLP, exemplifying its homogeneity of lung tissue density, and its preponderance of normally aerated units with normal $s\dot{V}$. In contrast, it also shows representative images of ZEEP-0.21, illustrating the emergence of a significant volume of lung with low $s\dot{V}$ within the poorly aerated density category, i.e. with both low $s\dot{V}$ (poorly ventilated) and poor aeration. It also shows images of ZEEP-1.0.

Table 1 Gas exchange parameters and respiratory variables.

	OLP	ZEEP-1.0	ZEEP-0.21
pH	7.34 ± 0.1	7.22 ± 0.2	7.29 ± 0.1
PaO_2/F_IO_2	423* ± 46.5	328.7 ± 131.3	227.9 ± 61.4
$PaCO_2$	41.8 ± 8.0	71.7 ± 32.4	55.1 ± 14.8
HCO_3^-	22.3 ± 3.1	26.2 ± 4.3	24.9 ± 2.1
V_T	3.8 ± 0.8	3.6 ± 0.5	3.6 ± 0.5

Values presented are means ± SD. *$P < 0.05$ vs. ZEEP-0.21. PEEP, positive end-expiratory pressure; F_IO_2, inspired fraction of oxygen; OLP, PEEP 12 cmH_2O and F_IO_2 1.0; ZEEP-1.0, PEEP = 0 cmH_2O and F_IO_2 1.0; ZEEP-0.21, PEEP = 0 cmH_2O and F_IO_2 0.21; pH, arterial pH; PaO_2/F_IO_2 (mmHg), ratio of partial pressure of arterial oxygen to the fraction of inspired oxygen; $PaCO_2$, arterial partial pressure of CO_2; HCO_3^-(mM), bicarbonate concentration; V_T (mL/kg), tidal volume

Discussion

We found that ZEEP together with low oxygen concentration increased the heterogeneity of both ventilation and lung tissue densities, likely fostering a greater amount of airway closure and ventilation inhomogeneities in poorly aerated lung regions. Conversely, OLP caused a more even distribution of aeration and of ventilation.

ZEEP-0.21 resulted in larger regions of both poor aeration and ventilation compared to OLP, whereas ZEEP-1.0 did not. The rate of absorption of gas from an unventilated region of the lung depends on the composition of the gas in that area when ventilation to it ceases, as well as the composition of the inspired gas.[25,26] When the inspired gas is 100% oxygen, the rate of collapse is faster than when air is breathed.[25,26] It has been demonstrated that if 100% oxygen is used, enough time of 'stable air trapping' is a prerequisite for lung collapse to occur.[26–32] 'Stable air trapping' here means no cyclic opening and closing of the distal airways.

If cyclic airway closure and reopening happen, no alveolar collapse would occur during a 10 min period unless the inspired ventilation–perfusion ratio (V_{AI}/Q) is extremely low (<0.01), in practice, indistinguishable from continuous closure. We purposely used small tidal volumes to avoid as much as possible cyclical opening and closing (i.e. tidal recruitment) of the small airways that would enable ventilation of these distal lung units. If 21% oxygen, small tidal volumes and ZEEP are used altogether, 'stable air trapping' is a plausible consequence.

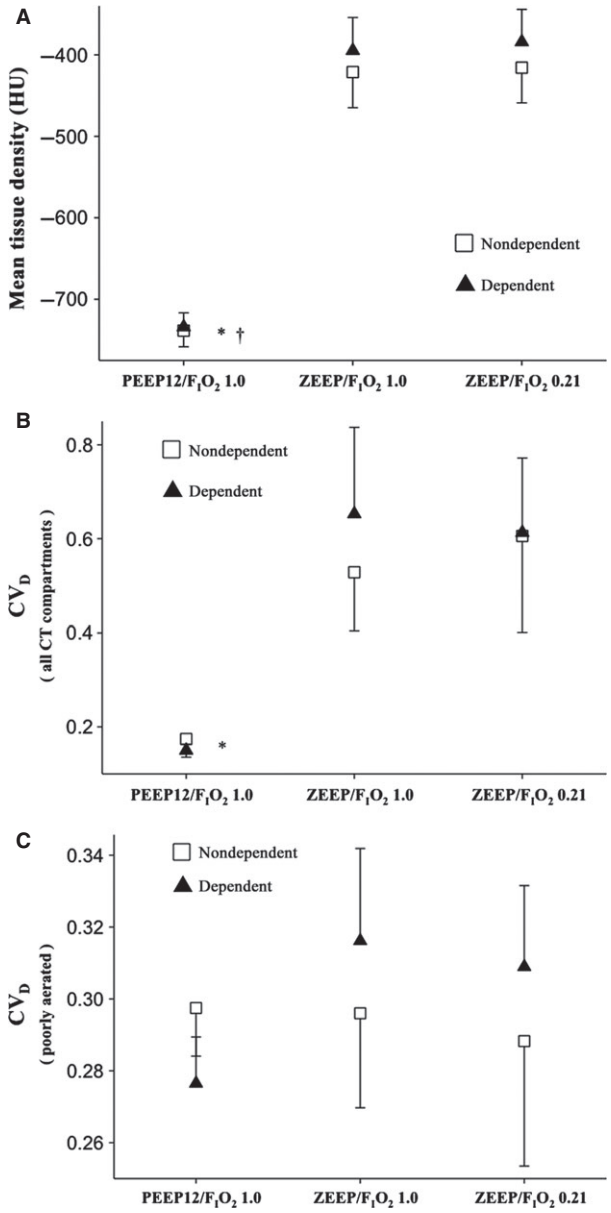

Low distending pressures and high F_IO_2 produced widespread dependent airway closure with subsequent absorption atelectasis in an experimental model of early ARDS, whereas low F_IO_2 substantially prevented atelectasis by much slower absorption of alveolar gas behind closed airways ('stable air trapping').[28] Besides the fact that now we studied healthy lungs, here we add the relevant information that the latter condition also entails a greater heterogeneity in specific ventilation distribution.

Rylander and coworkers[33] studied the size and distribution of the 'poorly aerated' density category in ARDS patients and concluded an uneven distribution of ventilation due to the presence of small-airway closure and/or obstruction. The behavior of the 'poorly aerated' density category in our data expressed also an uneven distribution of ventilation likely mainly due to the presence of small-airway closure and/or obstruction. Wellman et al.[34] have shown that patterns of ventilation heterogeneity are compatible with airway narrowing or closure in poorly aerated lung regions. They found that increased ventilation heterogeneity during mechanical ventilation with high tidal volume and zero PEEP occurs primarily at length scales <60 mm, with a significant component derived from subresolution (<12 mm) length scales. Components of specific ventilation heterogeneity at length scales of <12, 12–36, and 36–60 mm were highest in poorly aerated regions.

Fig. 1. Panel (A) *Mean tissue density*. In the analysis of the mean tissue density, we found a significant main effect for mechanical ventilation settings ($P = 0.003$) and for gravity level ($P = 0.028$). In the pairwise comparisons with a Bonferroni adjustment for multiple tests, the mean tissue density of Open Lung-PEEP (OLP) was significantly lower than Zero End-Expiratory Pressure (ZEEP) ZEEP-1.0 and ZEEP-0.21 (* and †, $P = 0.01$ and 0.012, respectively). FiO2 = fractional inspired oxygen. HU = Hounsfield units. Panel (B) *Coefficient of variation in lung densities for all CT categories*. The coefficient of variation (CV_D) of lung densities calculated for all density categories together was significantly lower on Positive End-Expiratory Pressure (PEEP) within both gravity levels (*, $P = 0.011$). Panel (C) *Coefficient of variation in lung densities for poorly aerated density category*. There was a statistically significant interaction between gravity level and mechanical ventilation settings on the coefficient of variation in lung densities calculated for the poorly aerated density category ($P = 0.013$). CV_D: coefficient of variation in lung densities; OLP: PEEP 12 cmH_2O and F_IO_2 1.0; ZEEP-1.0: PEEP = 0 cmH_2O and F_IO_2 1.0; ZEEP-0.21: PEEP = 0 cmH_2O and F_IO_2 0.21; white squares: nondependent level; black triangles: dependent level.

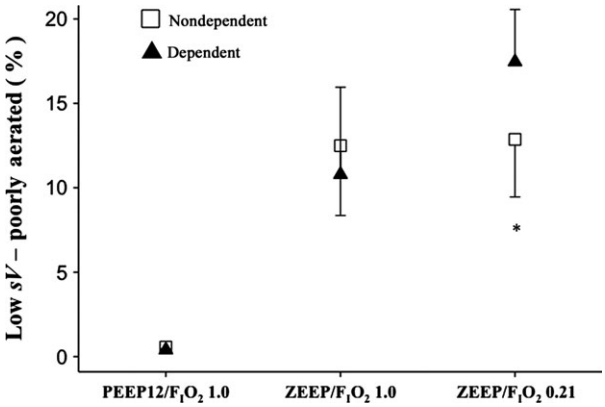

Fig. 2. *Volume of lung with low regional-specific ventilation within poorly aerated density category*. In the analysis of the volume of lung with low $s\dot{V}$ within the poorly aerated density category, a significant main effect for mechanical ventilation settings was found ($P = 0.008$). In the pairwise comparisons with a Bonferroni adjustment for multiple tests, the volume of lung with low $s\dot{V}$ within the poorly aerated density category of ZEEP-0.21 was greater than Open Lung-PEEP (OLP) (*, $P = 0.041$). OLP: Positive End-Expiratory Pressure (PEEP) 12 cmH_2O and F_IO_2 1.0; Zero End-Expiratory Pressure (ZEEP) ZEEP-1.0: PEEP = 0 cmH_2O and F_IO_2 1.0; ZEEP-0.21: PEEP = 0 cmH_2O and F_IO_2 0.21; white squares: nondependent level; black triangles: dependent level; $s\dot{V}$: regional-specific ventilation.

Similar size alveoli have been shown to deform very heterogeneously under uniaxial stretch[35] and even single cells deform differently due to variations in their stiffness.[36] Although it is still unclear how the acinar and alveolar geometry would change the distribution of forces and strains in a heterogeneous acinus, ventilation of such structure is prone to interfacial stress injury. Heterogeneity of regional lung mechanical properties produces different energy storages between neighbor structures,[37] which in turn may create damaging forces between neighboring units. This has an effect on regional ventilation and volume heterogeneity and would then be a possible cause of VILI. OLP can keep recruited lung regions and make stiffness more homogeneous at the length scales of small airways and alveoli,[34] and hence reduce the risk of injury development.

In the heterogeneously expanding lung, the very initial triggering mechanism of local injury and inflammation may occur predominantly in regions likely to undergo either concentration of stress or cyclic recruitment. By using dynamic PET with [^{18}F]-Fluoro-2-deoxy-D-glucose in a porcine model of VILI, we recently showed that inflammation was higher within the normally and poorly aerated lung regions than in overdistended or collapsed regions.[38] Besides the possibility of stress raisers at the intravoxel level (i.e. spots of accumulated tissue leveraging local stress), we can hypothesize other mechanisms explaining the marked inflammation in the poorly aerated density category: cyclic opening and closing of alveoli at the subvoxel level and cyclic opening and closing of small airways (also at subvoxel level) likely in poorly aerated regions with reduced specific ventilation, and increased tidal stretch, likely in normally aerated regions. The tidal opening and closing of distal bronchioles ('bronchiolotrauma' in analogy with the term atelectrauma) may be a key mechanism of VILI during mechanical ventilation. These findings reinforce and highlight the importance of better understanding of how ventilation heterogeneity is attenuated, exacerbated, and/or is modulated by the mechanical ventilation settings.

In an injured inhomogeneous lung, the stress and strain are unevenly distributed with local-

Fig. 3. *Representative images of OLP, ZEEP-0.21 and ZEEP-1.0.* Panel (A) This figure shows the homogeneity of lung tissue density, and the preponderance of normally aerated units with normal specific ventilation ($s\dot{V}$) at the Open Lung-PEEP (OLP) condition. And representative images of coincident poorly ventilation and poorly aeration during Zero End-Expiratory Pressure (ZEEP) ZEEP-0.21, showing the emergence of a significant volume of lung with low $s\dot{V}$ within the poorly aerated density category, i.e. with both low $s\dot{V}$ (poorly ventilated) and poor aeration. And representative images of ZEEP-1.0. First row of images: Tissue-density computed tomography image. Second row of images: Sample composite image showing the distribution of $s\dot{V}$ (1/min). Third row of images: Volume of lung within each aeration category (normally aerated, poorly aerated, and hyperinflated lung regions) divided into subcategories: no ventilation [$s\dot{V} < 0.5$/min]; low $s\dot{V}$ [$0.5/\text{min} < s\dot{V} < (\mu - 2\sigma)$]; normal $s\dot{V}$ [$s\dot{V} = \mu \pm 2\sigma$]; high $s\dot{V}$ [$(\mu + 2\sigma) < s\dot{V}$]. B) Each subcategory is expressed as percentage of the total lung volume within the image slice. The topographic distribution of lung regions defined as atelectatic, trapped, poorly aerated, normally aerated or hyperinflated is shown. Color scale indicates subregions with high, normal, or low $s\dot{V}$ within poorly aerated (High D = high density), normally aerated (Normal D = normal density), and hyperinflated (Low D = low density) categories. Open Lung-PEEP (OLP): Positive End-Expiratory Pressure (PEEP) 12 cmH_2O and F_IO_2 1.0; Zero End-Expiratory Pressure (ZEEP) ZEEP-1.0: PEEP = 0 cmH_2O and F_IO_2 1.0; ZEEP-0.21: PEEP = 0 cmH_2O and F_IO_2 0.21; $s\dot{V}$ = regional-specific ventilation. HU = Hounsfield units.

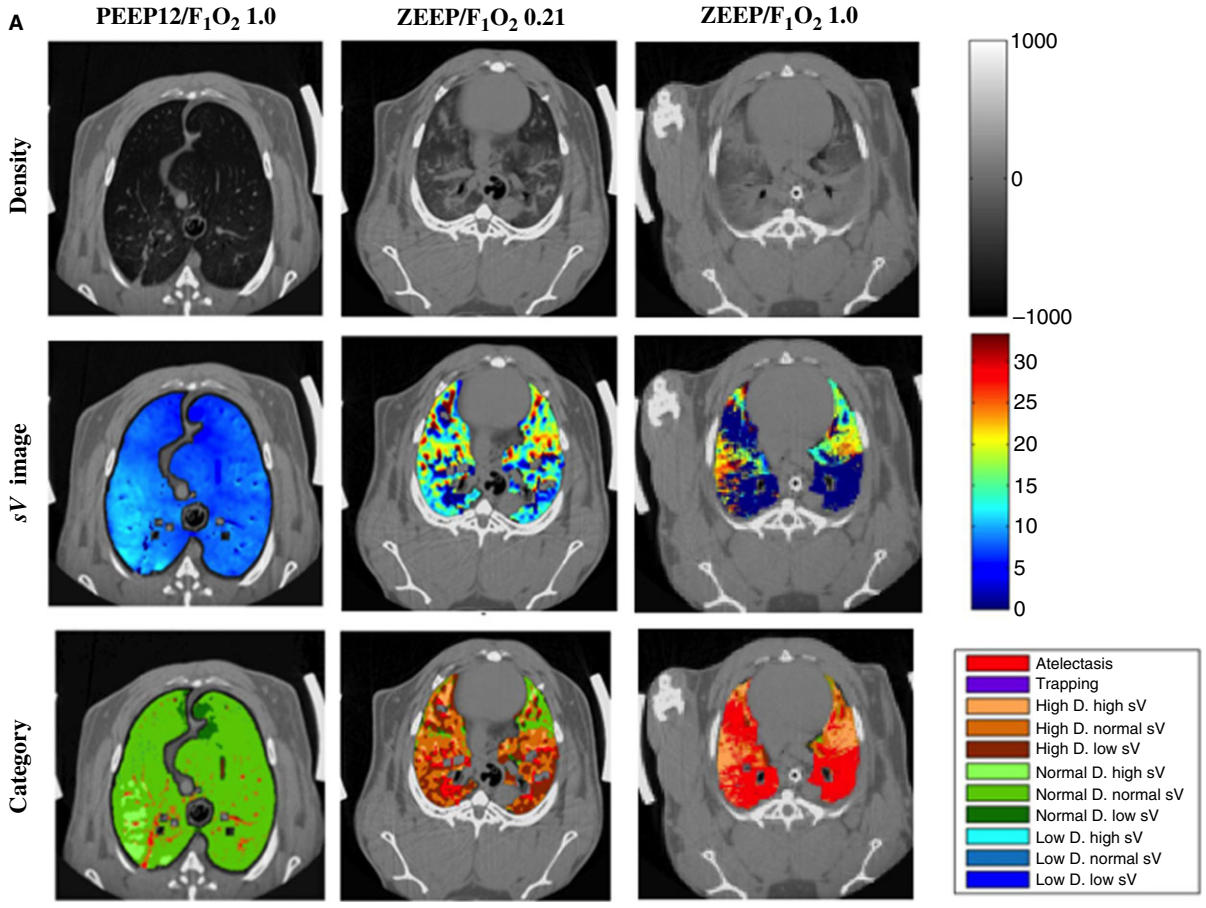

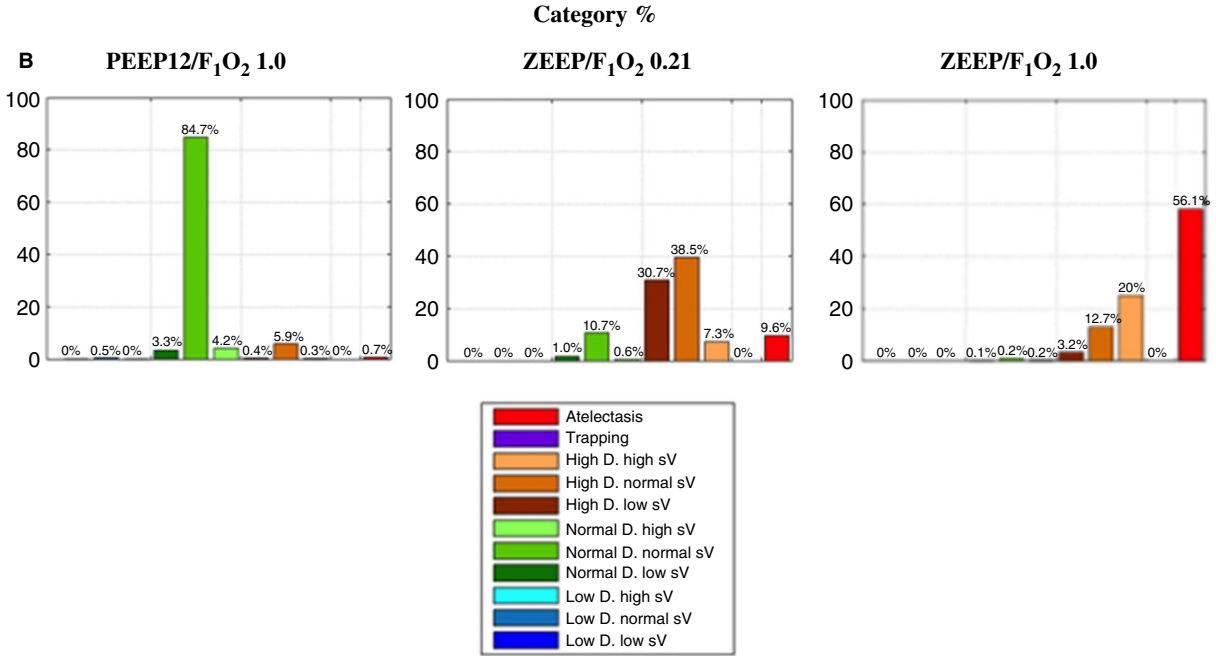

ized increase in stress.[39] The regional inhomogeneity may act as 'stress raisers'.[40] Cressoni et al. demonstrated that the lung inhomogeneities increased with ARDS severity, were positively associated with poorly aerated tissue, decreased when PEEP was increased, and were independently associated with outcome.[40] The physiological dead space is likely one of the strongest predictors of the ARDS outcome because it is related to the structural changes of the lung.[41] Cressoni et al. data exhibited that the only CT-scan-derived variable significantly associated with dead space fraction was the lung inhomogeneity extent. One can argue that this association between lung inhomogeneities with overall disease severity and mortality is meaningful only during ARDS and not in healthy lungs. However, the intensity of the lung inhomogeneities was similar in severe, moderate, and mild ARDS, and what actually changed between severe, moderate, and mild ARDS was only the extent of the lung inhomogeneities. The difference between patients with mild ARDS and patients with healthy lungs during major surgical procedures is likely also mainly a difference in the extent of the lung inhomogeneities. Another finding by Cressoni et al. was that the fraction of the poorly aerated tissue was well associated with the extent of inhomogeneity.

This study had several limitations. The technical aspects of analyzing structural and functional changes using KES imaging have been extensively discussed previously.[20] Given a potential difference in end-expiratory lung volume between PEEP of 12 cmH_2O and ZEEP and due to the fact that only two slices were analyzed, we cannot exclude that we analyzed different anatomical areas. The horizontal X-ray beam used for functional imaging in this study required that the animal be positioned vertically. This posture may slightly improve the respiratory mechanics in rabbit.[20] However, in this study, we compensated for this effect by raising the external pressure around the abdomen. Finally, this investigation was done in a small animal model.

In conclusion, in healthy lungs under mechanical ventilation, the present findings suggest that ZEEP together with low oxygen concentration promotes heterogeneity of ventilation and that of lung tissue densities, likely fostering a relevant amount of airway closure and ventilation inhomogeneities in poorly aerated lung regions. Furthermore, such heterogeneities can be minimized by OLP. The present data denote increased impedance of the subtending airways conducting gas to poorly aerated regions, either through narrowing or due to closure of these small airways, which may play a relevant role as potential early drivers of VILI.

References

1. Weiser TG, Regenbogen SE, Thompson KD, Haynes AB, Lipsitz SR, Berry WR, Gawande AA. An estimation of the global volume of surgery: a modelling strategy based on available data. Lancet 2008; 372: 139–44.
2. Arozullah AM, Khuri SF, Henderson WG, Daley J; Participants in the National Veterans Affairs Surgical Quality Improvement Program. Development and validation of a multifactorial risk index for predicting postoperative pneumonia after major noncardiac surgery. Ann Intern Med 2001; 135: 847–57.
3. Khuri SF, Henderson WG, DePalma RG, Mosca C, Healey NA, Kumbhani DJ; Participants in the VA National Surgical Quality Improvement Program. Determinants of long-term survival after major surgery and the adverse effect of postoperative complications. Ann Surg 2005; 242: 326–41–discussion 341–3.
4. Dos Santos CC, Slutsky AS. Invited review: mechanisms of ventilator-induced lung injury: a perspective. J Appl Physiol 2000; 89: 1645–55.
5. Serpa NA, Cardoso SO, Manetta JA, Pereira VGM, Espósito DC, de Pasqualucci MOP, Damasceno MCT, Schultz MJ. Association between use of lung-protective ventilation with lower tidal volumes and clinical outcomes among patients without acute respiratory distress syndrome: a meta-analysis. JAMA 2012; 308: 1651–9.
6. Lellouche F, Dionne S, Simard S, Bussieres J, Dagenais F. High tidal volumes in mechanically ventilated patients increase organ dysfunction after cardiac surgery. Anesthesiology 2012; 116: 1072–82.
7. Gajic O, Dara SI, Mendez JL, Adesanya AO, Festic E, Caples SM, Rana R, St SJ, Lymp JF, Afessa B, Hubmayr RD. Ventilator-associated lung injury in patients without acute lung injury at the onset of mechanical ventilation. Crit Care Med 2004; 32: 1817–24.

8. Jia X, Malhotra A, Saeed M, Mark RG, Talmor D. Risk factors for ARDS in patients receiving mechanical ventilation for > 48 h. Chest 2008; 133: 853–61.
9. Futier E, Constantin J-M, Paugam-Burtz C, Pascal J, Eurin M, Neuschwander A, Marret E, Beaussier M, Gutton C, Lefrant J-Y, Allaouchiche B, Verzilli D, Leone M, De Jong A, Bazin J-E, Pereira B, Jaber S; IMPROVE Study Group. A trial of intraoperative low-tidal-volume ventilation in abdominal surgery. New England J Med 2013; 369: 428–37.
10. Emr B, Gatto LA, Roy S, Satalin J, Ghosh A, Snyder K, Andrews P, Habashi N, Marx W, Ge L, Wang G, Dean DA, Vodovotz Y, Nieman G. Airway pressure release ventilation prevents ventilator-induced lung injury in normal lungs. JAMA Surg 2013; 148: 1005–12.
11. Levitt JE, Matthay MA. Clinical review: early treatment of acute lung injury - paradigm shift toward prevention and treatment prior to respiratory failure. Crit Care 2012; 16: 223.
12. Lipes J, Bojmehrani A, Lellouche F. Low tidal volume ventilation in patients without acute respiratory distress syndrome: a paradigm shift in mechanical ventilation. Crit Care Res Pract 2012; 2012: 416862.
13. Villar J, Slutsky AS. Is acute respiratory distress syndrome an iatrogenic disease? Crit Care 2010; 14: 120.
14. Determann RM, Royakkers A, Wolthuis EK, Vlaar AP, Choi G, Paulus F, Hofstra J-J, de Graaff MJ, Korevaar JC, Schultz MJ. Ventilation with lower tidal volumes as compared with conventional tidal volumes for patients without acute lung injury: a preventive randomized controlled trial. Crit Care 2010; 14: R1.
15. Futier E. Positive end-expiratory pressure in surgery: good or bad? Lancet 2014; 384: 472–4.
16. The PROVE Network Investigators, for the Clinical Trial Network of the European Society of Anaesthesiology. High versus low positive end-expiratory pressure during general anaesthesia for open abdominal surgery (PROVHILO trial): a multicentre randomised controlled trial. Lancet 2014; 384: 495–503.
17. Union EPATCOTE. Directive 2010/63/EU of the European Parliament and of the Council of 22 September 2010 on the protection of animals used for scientific purposes. Official J Eur Union 2010; 276: 33–79.
18. Bayat S, Porra L, Suhonen H, Nemoz C, Suortti P, Sovijärvi ARA. Differences in the time course of proximal and distal airway response to inhaled histamine studied by synchrotron radiation CT. J Appl Physiol 2006; 100: 1964–73.
19. Bayat S, Le Duc G, Porra L, Berruyer G, Nemoz C, Monfraix S, Fiedler S, Thomlinson W, Suortti P, Standertskjöld-Nordenstam CG, Sovijärvi AR. Quantitative functional lung imaging with synchrotron radiation using inhaled xenon as contrast agent. Phys Med Biol 2001; 46: 3287–99.
20. Bayat S, Strengell S, Porra L, Janosi TZ, Peták F, Suhonen H, Suortti P, Hantos Z, Sovijärvi ARA, Habre W. Methacholine and ovalbumin challenges assessed by forced oscillations and synchrotron lung imaging. Am J Respir Crit Care Med 2009; 180: 296–303.
21. Monfraix S, Bayat S, Porra L, Berruyer G, Nemoz C, Thomlinson W, Suortti P, Sovijärvi ARA. Quantitative measurement of regional lung gas volume by synchrotron radiation computed tomography. Phys Med Biol 2005; 50: 1–11.
22. Porra L, Monfraix S, Berruyer G, Le Duc G, Nemoz C, Thomlinson W, Suortti P, Sovijärvi ARA, Bayat S. Effect of tidal volume on distribution of ventilation assessed by synchrotron radiation CT in rabbit. J Appl Physiol 2004; 96: 1899–908.
23. Porra L, Suhonen H, Suortti P, Sovijärvi ARA, Bayat S. Effect of positive end-expiratory pressure on regional ventilation distribution during bronchoconstriction in rabbit studied by synchrotron radiation imaging. Crit Care Med 2011; 39: 1731–8.
24. Bayat S, Porra L, Albu G, Suhonen H, Strengell S, Suortti P, Sovijärvi A, Peták F, Habre W. Effect of positive end-expiratory pressure on regional ventilation distribution during mechanical ventilation after surfactant depletion. Anesthesiology 2013; 119: 89–100.
25. Dale WA, Rahn H. Rate of gas absorption during atelectasis. Am J Physiol 1952; 170: 606–13.
26. Dantzker DR, Wagner PD, West JB. Instability of lung units with low VA/Q ratios during O2 breathing. J Appl Physiol 1975; 38: 886–95.
27. Hedenstierna G. Airway closure: nothing good during anesthesia. Minerva Anestesiol 2012; 78: 1193–5.
28. Derosa S, Borges JB, Segelsjö M, Tannoia A, Pellegrini M, Larsson A, Perchiazzi G, Hedenstierna G. Reabsorption atelectasis in a porcine model of ARDS: regional and temporal effects of airway closure, oxygen, and distending pressure. J Appl Physiol 2013; 115: 1464–73.
29. Joyce CJ, Baker AB, Kennedy RR. Gas uptake from an unventilated area of lung: computer model of

absorption atelectasis. J Appl Physiol 1993; 74: 1107–16.
30. Joyce CJ, Williams AB. Kinetics of absorption atelectasis during anesthesia: a mathematical model. J Appl Physiol 1999; 86: 1116–25.
31. Rothen HU, Sporre B, Engberg G, Wegenius G, Hogman M, Hedenstierna G. Influence of gas composition on recurrence of atelectasis after a reexpansion maneuver during general anesthesia. Anesthesiology 1995; 82: 832–42.
32. Rothen HU, Sporre B, Engberg G, Wegenius G, Reber A, Hedenstierna G. Prevention of atelectasis during general anaesthesia [see comments]. Lancet 1995; 345: 1387–91.
33. Rylander C, Tylén U, Rossi-Norrlund R, Herrmann P, Quintel M, Bake B. Uneven distribution of ventilation in acute respiratory distress syndrome. Crit Care 2005; 9: R165–71.
34. Wellman TJ, Winkler T, Costa ELV, Musch G, Harris RS, Venegas JG, Vidal Melo MF. Effect of regional lung inflation on ventilation heterogeneity at different length scales during mechanical ventilation of normal sheep lungs. J Appl Physiol 2012; 113: 947–57.
35. Brewer KK, Sakai H, Alencar AM, Majumdar A, Arold SP, Lutchen KR, Ingenito EP, Suki B. Lung and alveolar wall elastic and hysteretic behavior in rats: effects of in vivo elastase treatment. J Appl Physiol 2003; 95: 1926–36.
36. Azeloglu EU, Bhattacharya J, Costa KD. Atomic force microscope elastography reveals phenotypic differences in alveolar cell stiffness. J Appl Physiol 2008; 105: 652–61.
37. Perchiazzi G, Rylander C, Derosa S, Pellegrini M, Pitagora L, Polieri D, Vena A, Tannoia A, Fiore T, Hedenstierna G. Regional distribution of lung compliance by image analysis of computed tomograms. Respir Physiol Neurobiol 2014; 201: 60–70.
38. Borges JB, Costa ELV, Suarez-Sipmann F, Widström C, Larsson A, Amato M, Hedenstierna G. Early inflammation mainly affects normally and poorly aerated lung in experimental ventilator-induced lung injury*. Crit Care Med 2014; 42: e279–87.
39. Mead J, Takishima T, Leith D. Stress distribution in lungs: a model of pulmonary elasticity. J Appl Physiol 1970; 28: 596–608.
40. Cressoni M, Cadringher P, Chiurazzi C, Amini M, Gallazzi E, Marino A, Brioni M, Carlesso E, Chiumello D, Quintel M, Bugedo G, Gattinoni L. Lung inhomogeneity in patients with acute respiratory distress syndrome. Am J Respir Crit Care Med 2014; 189: 149–58.
41. Gattinoni L, Bombino M, Pelosi P, Lissoni A, Pesenti A, Fumalli R, Tagliabue M. Lung structure and function in different stages of severe adult respiratory distress syndrome. JAMA 1994; 271: 1772–9.